



Seismic deformation of varved sediments in southern Fennoscandia at 7400 cal BP



Antti E.K. Ojala^{a,*}, Jussi Mattila^a, Joonas Virtasalo^a, Jukka Kuva^a, Tomi P. Luoto^b

^a Geological Survey of Finland, P.O. Box 96, FI-02151 Espoo, Finland

^b Faculty of Biological and Environmental Sciences, Ecosystems and Environment Research Programme, University of Helsinki, Niemenkatu 73, FI-15140 Lahti, Finland

ARTICLE INFO

Keywords:

Lake
Varved sediment
Disturbance structures
Postglacial faulting
Holocene
Fennoscandia

ABSTRACT

Soft-sediment deformation structures are preserved in clastic-biogenic varves of the Lake Nurmijärvi sequence from central-southern Finland. Deformation structures include centimeter-scale folding and faulting structures and larger convolute bedding, which are separated from the overlying undisturbed varved section by a turbidite dated at 7400 cal BP. The soft-sediment deformation provides evidence for postglacial seismic activity ca. 3500 years after the deglaciation of the study area. By screening the sizes of potential source faults for the event, the maximum earthquake moment magnitudes associated with the deformation structures were constrained to $M_w \approx 5.1\text{--}6.9$ with realistic 40% rupture scenarios, or up to $M_w \approx 5.1\text{--}7.7$ if more conservative scenarios are considered. The results of the study thus indicate a relatively high-magnitude postglacial seismic event in southern Finland, which adds to the evidence that the postglacial seismic activity was not just restricted to northern Fennoscandia, but was a more widespread phenomenon. The age of the Lake Nurmijärvi seismic event further demonstrates that high-magnitude seismic activity was not restricted to a relatively short period after deglaciation, but the period of high-magnitude postglacial seismic activity was much longer than previously thought. By assessing the orientations of faults that are presently active and using available focal mechanism data, our results suggest that strike-slip faulting may be a more important mechanism for the generation of both present-day and postglacial earthquakes in southern Finland than reverse faulting, which should further be accounted for in the assessment of long-term seismic hazards.

1. Introduction

The Fennoscandian Shield has experienced high-magnitude ($M_w \approx 6.5\text{--}8.2$) late- and postglacial earthquakes attributable to the release of lithospheric stresses during and after the retreat of the Scandinavian Ice Sheet (SIS) (Wu et al., 1999; Svendsen et al., 2004; Lund et al., 2009). These magnitudes are much larger than can be observed in historical data or instrumental measurements (e.g. Ahjos and Uski, 1992), and the estimates are mostly based on the appearance of postglacial fault (PGF) ramps tens of kilometers long and up to 10 m high over landscapes in Finland, Sweden and Norway (Arvidsson, 1996; Lagerbäck and Sundh, 2008; Kukkonen et al., 2010; Olesen et al., 2013; Malehmir et al., 2015; Ojala et al., 2017a). Tectonic stresses arising from the mid-Atlantic ridge can be regarded as the main driving force for the postglacial earthquakes, but the triggering effect is related to the excessive horizontal flexural stresses generated during the stagnant SIS and flexure of the lithosphere and mantle beneath, which were released during the melting of the ice sheet (e.g. Wu et al., 1999; Lund, 2005; Lund et al., 2009). Interest in postglacial seismicity in terrestrial

Fennoscandia was recently boosted by the availability of LiDAR (light detection and ranging) digital elevation models (DEMs), which have enhanced the discovery and geomorphological analysis of PGF segments and other seismically-induced features, such as paleolandslides and subglacial deformation patterns of Quaternary sediments (Sutinen et al., 2014a, 2014b; Smith et al., 2014; Berglund and Dahlström, 2015; Mikko et al., 2015; Palmu et al., 2015; Ojala et al., 2017a, 2017b). Results indicate that the majority of known PGFs are located in northern Fennoscandia (Fig. 1), they are often thrust faults that represent the reactivation of older fault zones, and they generally strike in a SW-NE direction (Olesen et al., 1992; Munier and Fenton, 2004; Ojala et al., 2017a). Furthermore, numerous landslides are found in close proximity to PGFs in Sweden and Finland, suggesting a causal relationship between postglacial faulting and the formation of landslides (e.g. Kujansuu, 1972; Lagerbäck and Witschard, 1983; Lagerbäck and Sundh, 2008; Ojala et al., 2017b).

Studies on co-seismic formations and sediments, such as paleolandslides and marine/lacustrine sequences, are important because they provide indirect evidence of paleoseismicity and can often be dated

* Corresponding author.

E-mail address: antti.ojala@gtk.fi (A.E.K. Ojala).

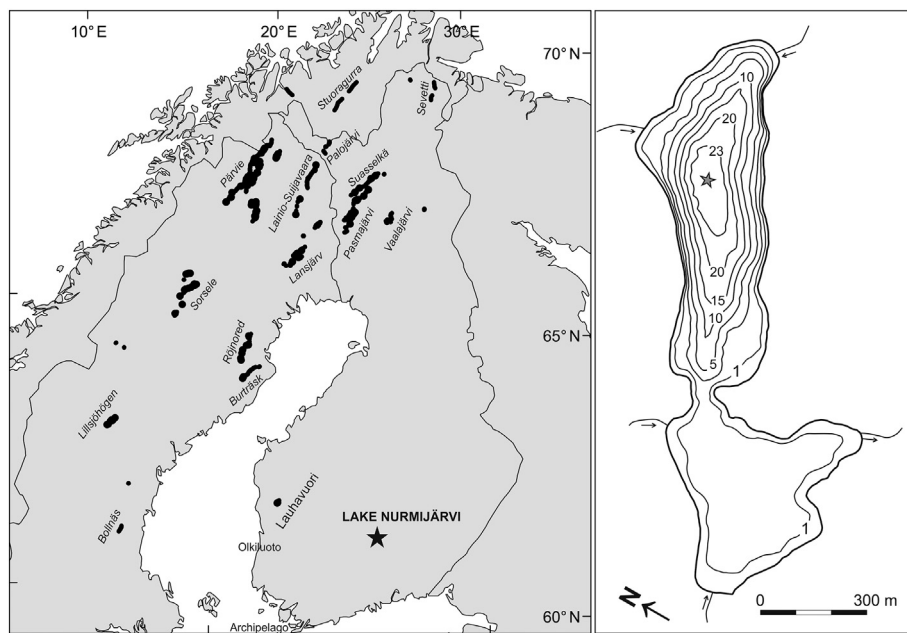


Fig. 1. Map indicating the location and bathymetry of Lake Nurmijärvi with the coring location marked with a gray star. The known postglacial faults (PGF) in northern Fennoscandia are indicated with black lines and named according to Lagerbäck (1990), Olesen et al. (2004, 2013) Lagerbäck and Sundh (2008), Mikko et al. (2015), and Palmu et al. (2015).

with better accuracy and precision than PGF scarps. Several investigations worldwide have demonstrated that the characteristics of aquatic sediments, such as deformation and faulting structures and turbidity current deposits, can be related to modern and historical earthquakes or interpreted as evidence for paleoearthquakes (e.g. Shilts and Clague, 1992; Monecke et al., 2006; Owen et al., 2011; Doughty et al., 2013; Strasser et al., 2013; Lajeunesse et al., 2017). Furthermore, well-dated sediment sections can provide continuous long-term records of paleoseismicity in the recently glaciated intra-cratonic areas, where primary evidence of postglacial faulting might be difficult to recognize due to the non-existent or thick overburden. For example, in Fennoscandia fine-grained sediments that were deposited in the Baltic Sea Basin (BSB) can reach several tens of meters in thickness on bedrock and glacial sediments.

Offshore seismic surveys in the southern Gulf of Bothnia, Archipelago Sea, and northern Baltic Sea Proper have revealed sediment disturbance structures such as faults and slumps, and characteristic chaotic to transparent seismic facies interpreted to be debris flow deposits (Hutri and Kotilanen, 2007; Hutri et al., 2007; Virtasalo et al., 2007). The slumps and debrites are focused on the same stratigraphic level, in the upper part of the glacial varved sediment unit. Virtasalo et al. (2007) dated the disturbance structures between 10,300 and 11,100 cal BP in the Archipelago Sea, whereas Hutri et al. (2007) dated them between 10,200 and 10,650 cal BP in the Olkiluoto area, which is 140 km or 500 clay-varve years in the direction of ice-margin retreat (Sauramo, 1923; Strömberg, 2005) (Fig. 1). The slumping and debris-flow deposition appear to be time-transgressive, and probably triggered by paleoseismic shaking that followed the retreating ice margin (Virtasalo et al., 2007). Such systematic searches are rare elsewhere in Fennoscandia, and those that exist indicate, for example, that the Pärvie PGF could not be identified with certainty beneath Lake Torneträsk in northern Sweden by Vogel et al. (2013). Jakobsson et al. (2014) and Smith et al. (2017), on the other hand, provided indirect evidence of PGFs in the glacial lacustrine sediments of lakes Vättern and Voxsjön, respectively, which they dated to the early Holocene, soon after deglaciation.

The currently studied Lake Nurmijärvi varved sediment in central-southern Finland was first discovered during the testing of high-resolution ^{137}Cs dating and diffusion of the cesium 1986 CE fallout peak from the Chernobyl nuclear disaster in the sequence (Ojala et al., 2017c). The same uppermost 50-cm-long sediment section was then

examined for its fossil chironomid communities and used to reconstruct past summer air temperature variability in the region (Luoto and Ojala, 2017). The results published by Luoto and Ojala (2017) showed that the principal variability in fossil chironomid assemblages correlated significantly with the meteorological data (air temperature), thus providing an exceptionally well-resolved record for Holocene climate changes. While opening the 7-m-long cores for further chironomid analysis, we discovered that the lower part of the core was separated from the upper section by a turbidite layer and that the lower part was strongly deformed by faulting and folding structures. Here, we present a description of these soft sediment deformation structures (SSDS), determine the timing for their formation using multiple dating methods, and discuss the relationship between sediment disturbance and paleoearthquake triggering in the context of postglacial paleoseismicity on the Fennoscandian Shield. This paper offers a perspective for seismic hazard assessment and on the timing and recurrence of postglacial seismicity in Fennoscandia.

2. Regional setting

Lake Nurmijärvi ($61^{\circ}35'\text{N}$, $25^{\circ}55'\text{E}$; 87.7 m a.s.l.) is a humic (water color 55–60 mg Pt L $^{-1}$) and mesotrophic (phosphorus 18–22 $\mu\text{g L}^{-1}$) boreal lake situated on the border of the municipalities of Sysmä and Hartola in central-southern Finland (Fig. 1). The lake has two sub-basins that are distinctively different in bathymetry and separated by a narrow, 1-m-deep sill (Fig. 1). The maximum depth of the oval-shaped NE basin is 23 m with a rather evenly flat area of about 100×250 m in the middle. Two inlets lead to the NE basin, supplying the lake with allochthonous mineral matter during the snowmelt season in spring (Ojala et al., 2017c).

The study area deglaciated during the early Holocene, about 11,000 cal BP. At that time, the highest shoreline of the Baltic Sea in the area was about 135 m above the present-day sea level (a.s.l.), but because of the emergence of the deglaciated terrain, Lake Nurmijärvi became isolated at around 9000 cal BP, during the postglacial (Ancylus) lake phase in the BSB history. Soon after isolation, the lake probably had a weak connection to the larger Lake Päijänne for a short period of time (Saarnisto, 1971; Ojala et al., 2005; Ojala et al., 2013). The Quaternary geology of the Lake Nurmijärvi catchment is characterized by bedrock outcrops covered by till and fine-grained deposits in relative equal proportions. The highest points of the bedrock reach over

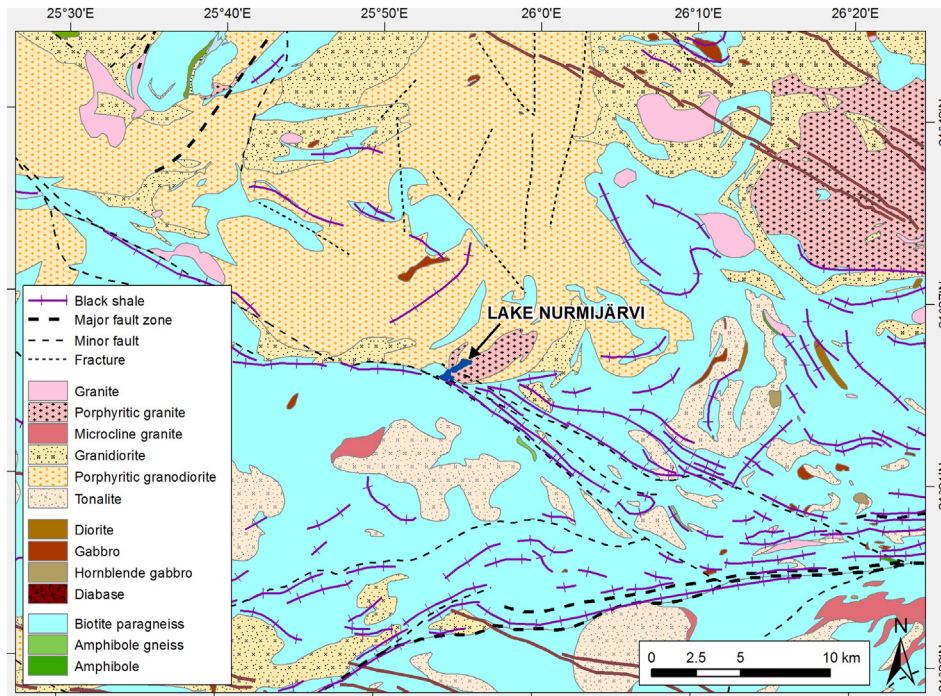


Fig. 2. Map showing the bedrock characteristics in the Lake Nurmijärvi area.

155 m a.s.l., whereas the lower-lying flat areas of fine-grained sediments on the SW and NE sides of the lake are mostly between 90 and 95 m a.s.l. Today, areas with fine-grained sediments are used as arable land.

The bedrock in the Nurmijärvi area is composed of Palaeoproterozoic metasedimentary and igneous rocks, and Lake Nurmijärvi is mostly located in a granitic unit, bounded in the north by a larger body of porphyritic granodiorite and in the south by biotite paragneiss (Fig. 2). In its southern part, the lake is located within the biotite paragneiss unit. A special feature north and south of the Lake Nurmijärvi area is the occurrence of NW–SE-striking diabase dikes, which emanate from the border of the Vibårg rapakivi massive located 70 km SE of Nurmijärvi, and which can be traced for a distance of about 140 km. There are no known postglacial faults in the study area, and in recent systematic LiDAR screening (Palmu et al., 2015), no indications of postglacial faults or landslides were found in the area. However, based on interpretations from airborne electromagnetic and magnetic maps, Lake Nurmijärvi is bounded in the south by NW–SE-striking faults (Fig. 2), which appear to be subsidiary faults to a major and segmented E–W-striking fault located south of Lake Nurmijärvi and which can be traced for a distance of at least 200 km. This fault is more or less parallel to the subvertical Somero Shear Zone (Väistönen and Skyttä, 2007), located 120 km south of Lake Nurmijärvi. The overall length of the NW–SE-traversing fault located just south of Nurmijärvi is about 100 km, but based on interpretations of geophysical data, the fault is highly complex and segmented and has further divided into several fault branches in its SE part.

According to the FenCat catalogue of earthquakes, the number of observed earthquakes in southern Finland is generally quite small (Fig. 3). The largest instrumentally-observed earthquake moment magnitudes are in the range of 4.5 and the mean moment magnitude is about 1.2. Approximately ten earthquakes have been recorded in the near-regional area of Lake Nurmijärvi in historical times (Fig. 3). The largest of these occurred in 1786 CE and had an estimated moment magnitude of $M_w \approx 2.9$, whereas the mean moment magnitude in the study area has been $M_w \approx 1.1$. The 1786 CE earthquake was also the closest observed earthquake to Lake Nurmijärvi and its estimated epicenter was located about 2 km from Nurmijärvi. It is not known which

of the faults in the area hosted these earthquakes or whether they were generated by blind faults not seen in the surface data. In southern Finland, the focal mechanisms of earthquakes generally indicate a combination of strike-slip and reverse faulting (Korja and Kosonen, 2015).

3. Materials and methods

The thickness and distribution of sediments in Lake Nurmijärvi has been investigated with acoustic sub-bottom profiling (Ojala et al., 2017c). The sediments in the oval-shaped 23-m-deep NE basin are composed of a distinctive and extensive succession of the clastic-biocenotic type of varves as presented in Ojala et al. (2017c) and Luoto and Ojala (2017), which are similar to those found in lakes Nautajärvi, Korttajärvi, Lehmilampi, and Kalliojärvi in southern Finland (e.g. Ojala et al., 2000; Ojala and Alenius, 2005; Haltia-Hovi et al., 2007; Saarni et al., 2016). The basic structure of the clastic-biocenotic type of varves is very simple. They consist of two laminae, a denser and pale-colored lamina of mineralogenic material and a darker lamina composed of biogenic material (e.g. Renberg, 1982; Ojala and Alenius, 2005; Zolitschka et al., 2015). The thickness of the clastic lamina is often linked to snowmelt intensity during spring, whereas the biogenic lamina represents summer to winter deposition from allochthonous and autochthonous sources (Ojala and Alenius, 2005; Haltia-Hovi et al., 2007; Saarni et al., 2016).

Altogether, five 40–80-cm-long surface sediment cores (NJ-P1 to NJ-P5) (Ojala et al., 2017c) and three parallel 690–700-cm-long gravity piston cores (Nurmij1 to Nurmij3) were obtained from the middle of the 23-m-deep basin in 2015 and 2016 (Fig. 1).

Physical analysis of the gravity piston cores included measurements of weight loss on ignition (LOI, calculated as the weight difference after drying at 105 °C overnight and ashing at 550 °C for 2 h) and magnetic susceptibility with a Bartington Instruments MS2E1 sensor at 1-cm resolution. The opened core halves were carefully cleaned and photographed to enable a description of the sediment structures, varve counts, and varve thickness analysis of the uppermost 50 cm using line-scan image analysis as presented in Ojala et al. (2017c). Correlation between parallel core sequences was based on magnetic susceptibility

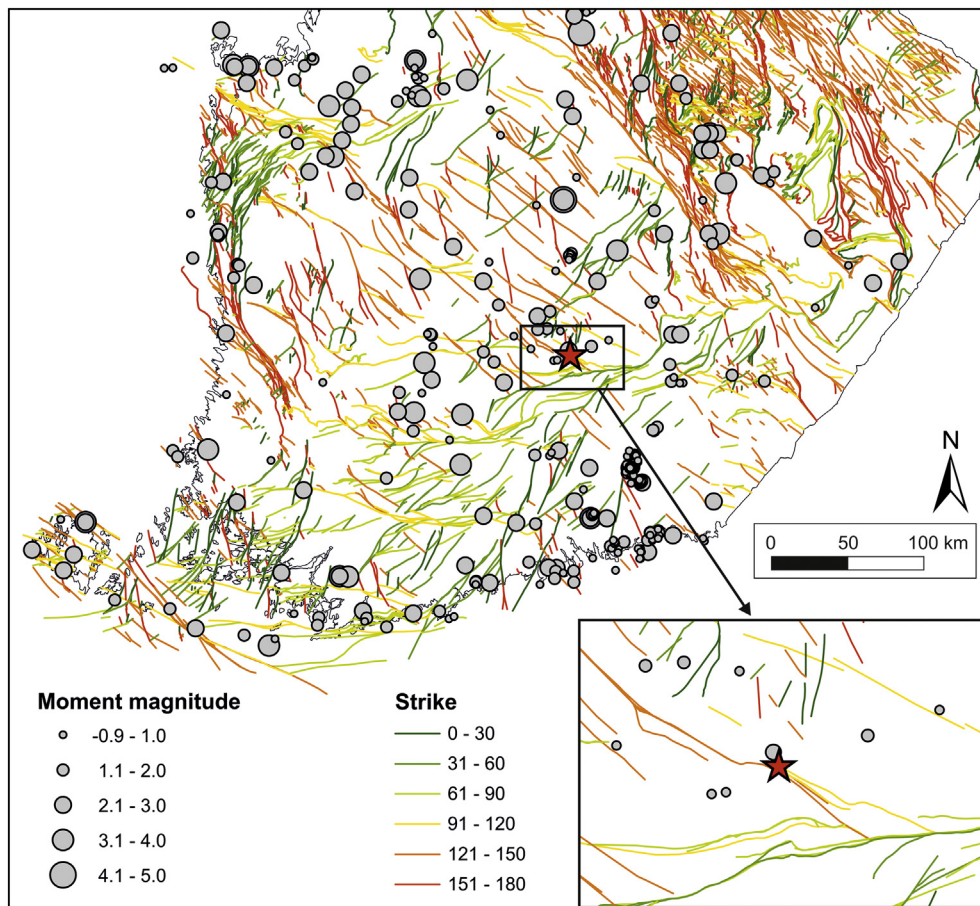


Fig. 3. Map of faults and recent earthquakes in southern Finland. The location of Lake Nurmijärvi is indicated with a red star. (For interpretation of the references to color in this figure legend, the reader is referred to the web version of this article.)

and a detailed stratigraphic description, in which distinct marker laminae played a significant role.

Sections of full cores were scanned with computed X-ray tomography prior to splitting into core halves to test the capability of the instrument in documenting millimeter-scale laminae structures of the clastic-biogenic type of varves through unopened plastic core liners of 70 mm in diameter. The equipment used was a GE phoenix v|tome|x s with a $400 \times 400 \text{ mm}^2$ 4 MPix detector. The best achievable resolution that contained almost the whole core horizontally was $24.37 \mu\text{m}$. With this resolution, one field of view (FOV) was 48.74 mm horizontally and only 39 mm vertically. To achieve a combination of a fast scanning time, good resolution and a large field of view, we used the fast|scan module, in which the sample rotates continuously and images are taken “on the fly”, and the multi|scan module, taking eight FOVs vertically, which were then stitched together. We used an accelerating voltage of 75 kV and a current of $320 \mu\text{A}$, taking 1199 projections with a 500-ms exposure time for each FOV, adding up to a total scan time of 1 h and 20 min for a total length of 291 mm along the core. 3D reconstruction and stitching were carried out with GE datos|x 2 rec, using the multi|scan module.

In addition, buried brownish Fe hydroxide crusts were sampled from the fresh core surface, and analyzed for elemental composition using a JEOL JSM5900LV low-vacuum scanning electron microscope (SEM) coupled to an Oxford 7274 energy dispersive X-ray micro-analyzer (EDS).

Dating of the Nurmijärvi sediment sequence was based on varve counts and measurements of the cesium (^{137}Cs) content with an EG&G Ortec ACE™-2K (four-inch NaI(Tl) detector) and fully digital BrightSpec bMCA-USB pulse height analyzer (coupled to a well-type NaI(Tl)

detector), as presented in Ojala et al. (2017c), and the determination of decadal to centennial directional changes in the Earth's magnetic field recorded in sediments and referred to as paleomagnetic secular variation (PSV). The method and the Holocene PSV reference curves ('master curves') for Fennoscandia have been presented in Ojala and Tiljander (2003) and Snowball et al. (2007). While Ojala et al. (2017c) earlier cross-correlated the relative declination variations of the uppermost 75 cm with the Lake Nautajärvi reference curve (Ojala and Tiljander, 2003) and instrumentally observed features for southern Finland (Nevanlinna, 1979) and Poland (Wardinski, 2007) for the last 400 years, here we extended the PSV measurements to cover the entire 700-cm-long sequence. Palaeomagnetic samples were taken into 7 cm^3 polystyrene cubes at 3-cm resolution for PSV measurements conducted at the Geological Survey of Finland with a 2G Enterprises SRM-755-4K tri-axial SQUID magnetometer. Representative samples from several depth levels were selected for stepwise alternating field (AF) demagnetization (5 to 120 mT peak AF) to test the stability of the NRM. The remaining samples were demagnetized with 20 mT peak AF and re-measured.

4. Results and interpretation

Published results for Holocene PSV of the Earth's magnetic field obtained from varved lake sediments demonstrate that clastic-biogenic varves are exceptionally suitable for paleomagnetic dating and can provide regionally applicable reference curves for stratigraphic correlation and age control in northern Europe (Ojala and Tiljander, 2003; Snowball et al., 2007). Variations in natural remanent magnetization (NRM) of declination and inclination in the Lake Nurmijärvi sequence

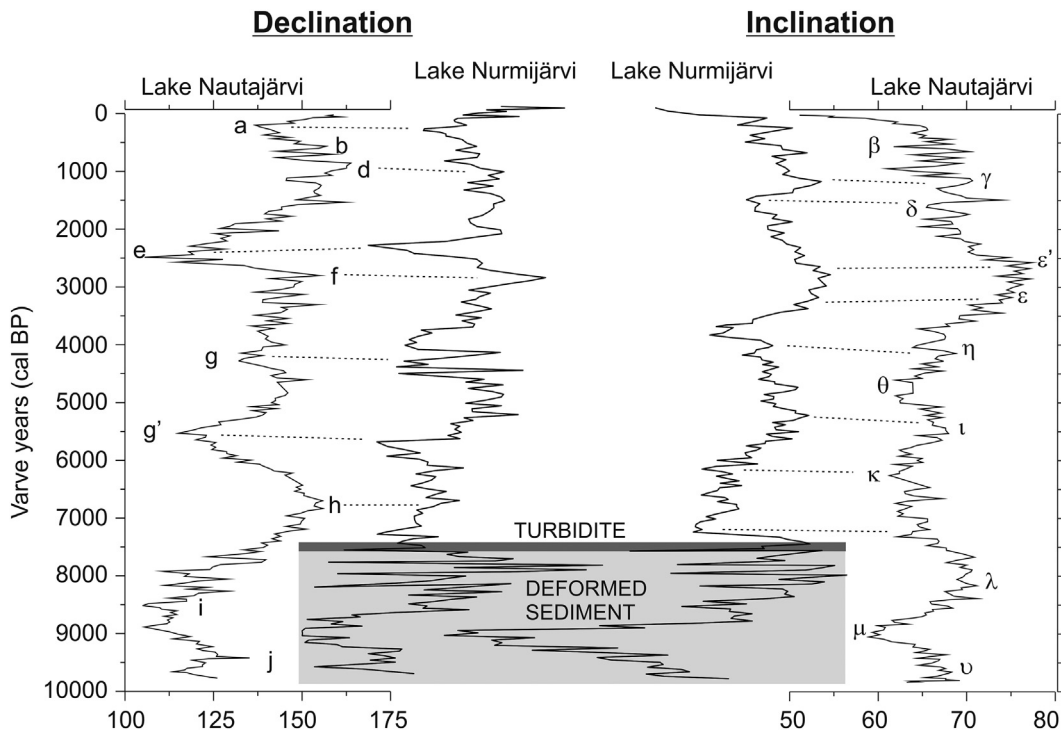


Fig. 4. Records of NRM declination and inclination from Lake Nurmijärvi compared with Lake Nautajärvi varve-dated reference curves. Characteristic features of the NRM signal are connected with scattered lines and shaded gray areas indicate sections with turbidite (darker gray) and disturbed varves (lighter gray).

are presented and correlated with the Lake Nautajärvi varve-dated reference curve in Fig. 4.

The magnetic signal of the Lake Nurmijärvi sequence is dominated by a relatively high concentration of pseudo-single-domain and stable single-domain magnetite and characterized by a strong and stable primary component of the magnetic direction (Ojala et al., 2017c). Patterns of NRM variation are highly consistent with the NRM records of Lake Nautajärvi, in which declination features a, d, e, f, g, g', and h, and inclination features γ , δ , ϵ , ϵ' , η , θ , ι , and κ are well represented. This correspondence provides a good basis for assigning PSV ages for the uppermost 490 cm of the Lake Nurmijärvi sediment sequence, and dating is based on matching of these relatively evenly spaced features. However, below the turbidite layer at 490 cm, the stable signal of NRM declination and inclination dramatically scatters, probably because of the deformed character of the sediment (see sediment description below). As a consequence, PSV dating of the Lake Nurmijärvi sequence is limited to this depth.

The age-depth curve of the Lake Nurmijärvi sequence is presented in Fig. 5. In addition to patterns of NRM for the entire sequence, the dating is based on repeated varve counts of the uppermost 50 cm (250 ± 5 varves), the vertical distribution of ^{137}Cs , and PSV comparison with instrumental observations as presented in Ojala et al. (2017c). The accuracy of the present age-depth curve is based on errors associated with the Nurmijärvi varve chronology ($\pm 2\%$), the reference curve varve chronology ($\pm 1\%$) (Ojala and Tiljander, 2003), the sampling resolution of paleomagnetic cubes (here 20–40 years), and errors associated with the correlation of PSV records. In addition, studies by Ojala and Tiljander (2003) and Ojala et al. (2017c) indicate that with clastic-biogenic varves, the NRM signal is fairly rapidly locked in due to capping, efficient burial, and compaction of the sediment by spring snowmelt-derived mineral matter. They considered that the so-called lock-in delay of depositional remanent magnetization would be of 5–20 years in magnitude with sediments of this type. When put together, we estimate that the age of the turbidite layer at the depth of 490–495 cm in the Lake Nurmijärvi section is $7400 \text{ cal BP} \pm 150$ years (2% error estimate), providing an average rate of deposition (varve

thickness) of about 0.66 mm a^{-1} for this period.

A composite sedimentary record from Lake Nurmijärvi is presented in Fig. 6. The section is continuously laminated with clastic-biogenic varves. The annual nature of varves was verified with independent dating methods (^{137}Cs , PSV) (Ojala et al., 2017c), and their character and composition is similar to varved records in comparable catchment settings in Finland and Sweden (e.g. Ojala et al., 2000; Ojala and Alenius, 2005; Haltia-Hovi et al., 2007; Saarni et al., 2016). The fine texture varves indicate an anoxic deposition environment on the lake bottom, where suspended mineral-rich material is seasonally transported by ditches that drain the catchment during flooding episodes. Varves can only appear in the absence of post-depositional erosion, resuspension, bioturbation, seismic liquefaction, bubbling of gases, and gravity-induced sediment relocation (Zolitschka et al., 2015).

The lithology of Lake Nurmijärvi varves is different for the uppermost 30 cm (the last 100 years), where an overwhelming imprint of anthropogenic activity in the catchment has substantially increased the rate of allochthonous mineral matter influx, as well as the deposition of Fe monosulfide sediment due to an increase in primary production and prolonged seasonal anoxia (see Ojala et al., 2017c; Luoto and Ojala, 2017). Below 30 cm, the sediments are more pristine and consist of less mineralogic matter and thinner varves, although decadal to centennial variations in varve thickness are evident.

The perfectly horizontal and undisturbed section of clastic-biogenic varves spans between the sediment surface and the depth of 490 cm. Between 490 and 495 cm appears a 5-cm-thick light-colored layer having an undulating erosional basal contact that cuts the underlying laminae (Fig. 6A, B). The basal contact is overlain by silty clay that fines upward to a thin pale clayey top layer. No sedimentary structures such as parallel and ripple cross-lamination are observed in addition to the overall fining-upward grain size. This structure corresponds to the classical turbidite facies T_a and T_e after Bouma (1962). The upper fine-grained succession (T_e) is subdivided into the T_6 and T_7 facies of fine-grained turbidites according to Stow and Shanmugam (1980). This sequence is typical of well-documented seismically triggered turbidites in Alpine lakes (Strasser et al., 2013). It results from shallow erosion by

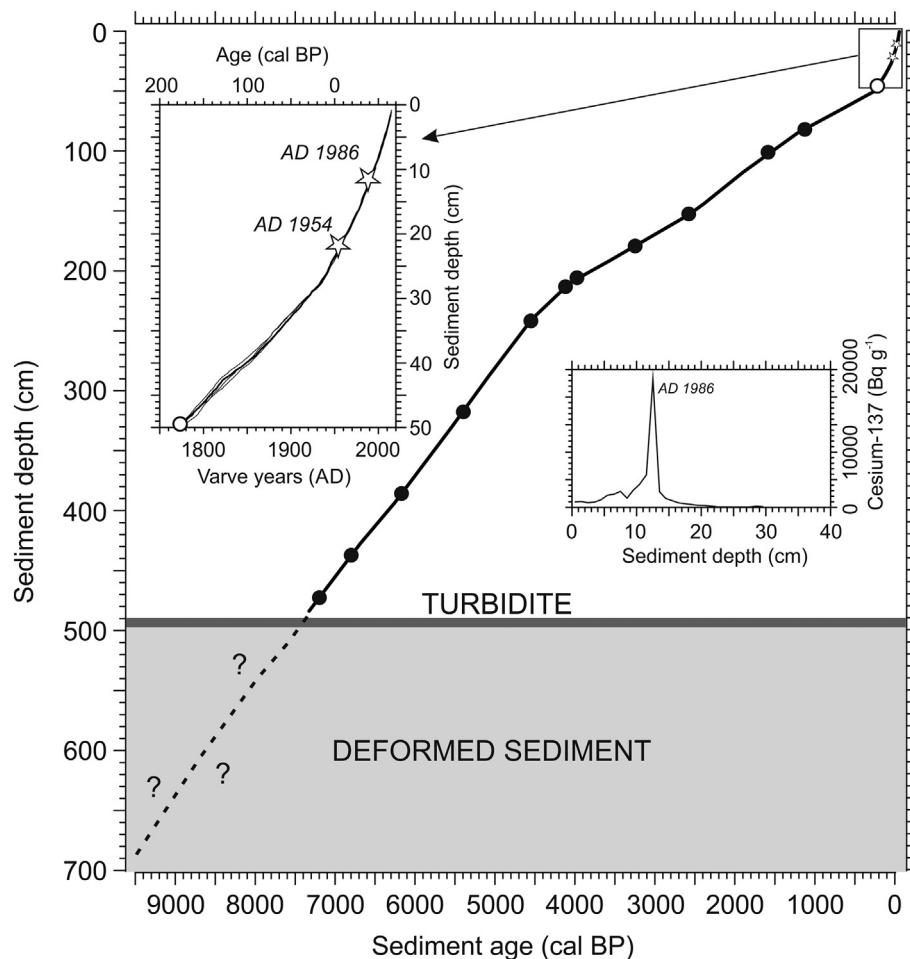


Fig. 5. Age–depth model for the Lake Nurmijärvi composite sequence based on varve chronology, ^{137}Cs stratigraphy, and paleomagnetic dating. Black and white circles represent tie-points of declination and inclination PSV curves between the Lake Nurmijärvi data and the Lake Nautajärvi reference curves (see Fig. 4) and instrumental observations (Ojala et al., 2017c), which provide a basis for the Lake Nurmijärvi age–depth model. Shaded gray areas indicate sections with turbidite (darker gray) and disturbed varves (lighter gray).

and subsequent deposition from a low-density turbidity current, which rapidly decelerates as it reaches the flat basin plane of the lake so that the deposits do not preserve the full sequence of turbidite facies divisions described by Bouma (1962) and Stow and Shanmugam (1980). The flows are typically triggered at shallow lake margins, where seismic shaking brings sediment particles into suspension, which then begins to flow under its own gravity along the lake floor.

Below the turbidite layer, the lowermost two meters of the Nurmijärvi sequence are characterized by different types of soft-sediment deformation structures (SSDS) that are clearly post-depositional in origin (Fig. 6). The degree and type of SSDS is uniform in parallel sediment core sections and they occur at exactly the same depth (same marker horizons), indicating that these deformations are not due to sediment coring or sampling. The typical SSDS that are seen in varves are fractures, faulting and folding microstructures, and convolute laminae.

Fractures and cracks are easily detected in the fresh sediment surface because they often have a brownish mineral crust. Based on SEM-EDS analyses, this brownish crust material is predominantly composed of iron and oxygen, with traces of silicon, sulfur, phosphorus, and aluminium (Table 1). The crust mineralogy is interpreted to be ferric hydroxide, which commonly forms at oxic–anoxic interfaces in sediments (Mortimer, 1942; Deike et al., 1997) and may bind dissolved phosphorus (Lijklema, 1980). The Si, Al, and S present probably represent admixed sediment particles such as clay minerals and Fe monosulfide in the crusts. Iron hydroxide crusts are also clearly visible

in X-ray tomography because of their higher density compared to sediment the matrix (Fig. 7).

Fault microstructures are typical SSDS in the upper part of the deformed sediment section (depth of about 500–600 cm). They are well detected because of varves and the appearance of distinct marker horizons. Fault displacement is typically 1–3 cm (Fig. 6C–E), and fault planes that cross-cut varves are often filled with ferric hydroxide, indicating post-depositional infiltration of sediment pore water. Even though the cores were not oriented, the fault planes are systematically oriented with respect to folding and with a dip angle of around 60°. Faults are associated with folding structures that indicate more plastic deformation. The varved structure indicates a folding dimension of up to 3–5 cm and folding is sometimes associated with flame-like structures (Fig. 6F, E). The flame-structures are comparably rare, however, probably because the sediment was already compacted at the time of disturbance.

Compared with photographs of the fresh sediment surface, the image taken with X-ray tomography displays a millimeter-scale clastic-biogenic varve structure as well as folding and faulting characteristics exceptionally well (Fig. 7). It meets all the requirements for varve structural analysis, as well as manual or semi-automated varve counting and thickness measurements. Where varve counting would previously have been conducted from opened and often epoxy-impregnated samples, X-ray tomography provides a new rapid tool for sub-millimeter-scale varve analysis without splitting the sediment cores. Computed X-ray tomography also opens new perspectives for varve and sediment

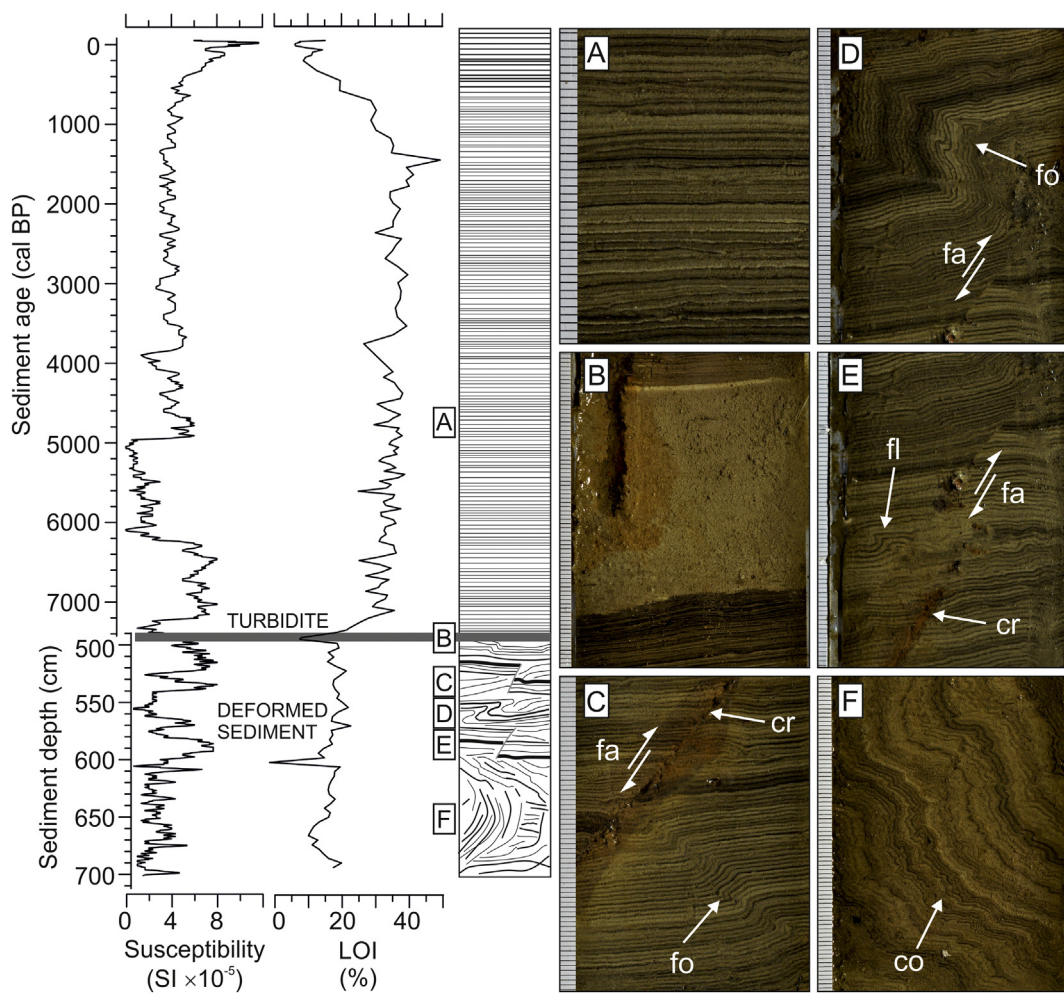


Fig. 6. The upper part of the Lake Nurmijärvi sequence exhibits perfectly horizontal and undisturbed clastic-biogenic varves (A) and a single turbidite layer at the depth of 490–495 cm (B). The disturbed lower part of the Lake Nurmijärvi sequence is composed of folding (fo) and faulting (fa) microstructures (C, D, E), fractures and cracks (cr) (C, E), and convolute bedding (co) with characteristics of sediment liquefaction (F).

Table 1
Composition (%) of the fracture mineral crust as measured by SEM-EDS.

Spot ID	O	Al	Si	P	S	Fe
1	77.47	n.d.	2.16	n.d.	1.05	19.32
2	76.73	0.32	2.08	0.29	0.96	19.62
3	79.63	n.d.	2.18	0.3	1.09	16.79
4	78.17	0.41	2.92	0.78	0.96	16.77
5	80.09	n.d.	2.05	0.26	0.86	16.73
6	75.56	0.6	3.5	0.76	0.77	18.81
7	77.09	0.38	1.97	1.14	0.8	18.62
8	75.16	n.d.	2.21	0.97	0.91	20.74
9	76.73	0.4	1.8	1.33	0.85	18.99
Mean	77.39	0.42	2.32	0.73	0.092	18.49
Std. dev.	1.67	0.11	0.54	0.41	0.11	1.43
N	9	5	9	8	9	9

at.%, percentage of atom quantity, n.d. = not detected, N = number of analyses.

structure analysis via 3D modeling.

The lower part of the disturbed section (depth of about 600–700 cm) displays asymmetric and disharmonic folding and convolute laminae structures where varves are orientated in an almost upright position (Fig. 6F). Even with heavily contorted deformation, the varve structure with seasonal laminae can still be detected, which indicates that the sediments did not originate from gravity-induced down-slope transport and re-deposition of littoral material. Apart from the turbidite layer at

490–495 cm, the depositional modification of profundal sediments of the Lake Nurmijärvi sequence by slumps and hyperpycnal currents is negligible.

5. Discussion

5.1. Earthquake-induced deformation structures

Soft-sediment deformation structures are features of unconsolidated water-saturated sediments that have a high susceptibility to liquefaction (Sims, 1973; Owen et al., 2011). They are known from a wide variety of deposition environments and are especially abundant in lacustrine successions because of the absence of hydrodynamic and sedimentary processes that could obliterate the products of deformation (Sims, 1973). SSDS can be induced by many processes, including gravity slumping, wave- and current-driven stresses, excessive loading or unequal loading, sudden changes in the groundwater level, biological and chemical agents, and earthquakes (Sims, 1973; Allen, 1982; Owen et al., 2011). According to a review by Shanmugam (2017), at least 120 different types of SSDS have been described worldwide, but those that are related to seismically-induced liquefaction or fluidization features are predominantly referred to seismites (Seilacher, 1969; Sims, 1973; Owen et al., 2011).

Considering the simple shape and relatively small size of the Lake Nurmijärvi basin, and in the absence of current-driven unequal loading and biological and chemical agents, we interpret that paleoseismicity is

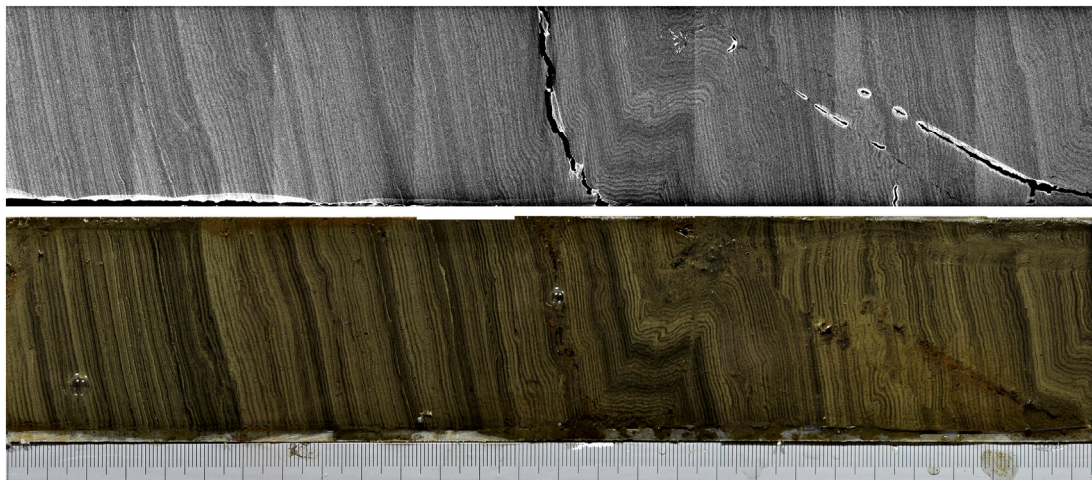


Fig. 7. A fresh sediment photograph (lower) and a cross-section of the 3D tomographic image (upper) of Lake Nurmijärvi clastic-biogenic varves. Lighter gray indicates higher density and darker gray lower density material in the X-ray tomography image.

the most probable triggering mechanism that formed SSDS in the sequence around 7400 cal BP. The seismic interpretation benefits from the fact that the Lake Nurmijärvi sequence is composed of millimeter-scale clastic-biogenic varves that are very pronounced and have similar characteristics for the undisturbed (0–490 cm) and disturbed (495–700 cm) sections, which are separated by a normally graded turbidite. Varves of this type are typical products of a stable and calm sediment deposition environment (e.g. Ojala and Alenius, 2005; Zolitschka et al., 2015). None of tens of well-described and in detail studied Holocene varved sections in Fennoscandia have reported such SSDS seen in the Lake Nurmijärvi sequence (e.g. Renberg, 1982; Ojala et al., 2000; Ojala and Tiljander, 2003; Ojala and Alenius, 2005; Haltia-Hovi et al., 2007; Snowball et al., 2007; Saarni et al., 2016). The occurrence of extensive macro- and microstructural deformation of varves ca. 1600 years after the isolation of the basin clearly indicates sudden post-depositional event.

The type of SSDS in the Nurmijärvi section is similar with those used as indicators of paleoearthquakes worldwide (e.g. Owen et al., 2011; Gràcia et al., 2013). More specifically, we recognize turbidite layer, convolute bedding, and smaller-scale *in situ* microstructures (faults and folds), which are all typical coseismic SSDS in lacustrine sediments (e.g. Allen, 1982; Monecke et al., 2006; Carillo et al., 2008; Beck, 2009). Faulting and folding microstructures seen in the Lake Nurmijärvi varves are similar with the earthquake-induced structures seen in Lake Le Bourget laminated sediments (Beck, 2009) and Seelisberg Seeli and Baldeggersee varves (Monecke et al., 2006). In addition, erosional features and multi-pulsed or stacked turbidites that would indicate hydrological changes, flooding frequencies, or repeated gravity-induced slumping are absent from the Lake Nurmijärvi sequence. The convolute bedding in the lower part of the Lake Nurmijärvi sequence indicates significant vertical movement of material with traces of plastic deformation (6 F). The disharmonic flame-like structures could indicate vibration of water-sediment mixtures. We related these structures to seismic shock according to Allen (1982) and Owen et al. (2011), although the extent of these deformations is difficult to determine from sedimentary cores alone.

We interpret that the turbidite in the Lake Nurmijärvi section was formed instantaneously after an earthquake brought sediment into suspension, which then generated a near-bottom turbidity current flowing to the deepest part of the lake, forming a 5-cm-thick layer. At the same time, the varved sediments that had already been deposited underwent considerable structural deformation due to shaking of the lake bottom, where the largest convolute bedding was formed deeper in the sediment and faulting and folding microstructures closer to the sediment surface (Fig. 6). We emphasize that the presence of a single

turbidite layer and an undisturbed section of clastic-biogenic varves since 7400 cal BP points to a single paleoseismic event at 7400 cal BP rather than a creeping type of movement or recurrence of a paleoearthquake, which is typical for basin-wide turbidites triggered by strong seismic shaking (e.g. Moernaut et al., 2014).

5.2. Fault instability

There are no direct indications of which fault could have been active and generated the soft-sediment deformation structures in the Lake Nurmijärvi section, and in order to make an estimate of the source area and potential host faults for the event, we therefore examined the general patterns of seismicity in southern Finland. This is based on the assumption that during the postglacial period, the retreat of the ice sheet and associated stress changes merely acted as a trigger and reduced the stability of zones that are already highly unstable in the present-day stress state (Hökmark and Fälth, 2014), and the current stress state and earthquake activity can thus be applied in the search for zones potentially unstable in the postglacial period. This hypothesis is supported by evidence that the postglacial faults in northern Scandinavia are also active in the present-day stress regime (e.g. Lagerbäck, 1990; Lindblom and Lund, 2011; Olesen et al., 2013; Uski et al., 2003).

In the analysis, we first computed the average strike values (values between 0 and 180°) for each fault on the geological map and associated these strike values with the FenCat fault database. The derived strike values are presented with different colors in Fig. 3. In order to gain an idea of which fault each earthquake epicenter given in the FenCat catalogue was associated with, we carried out a spatial analysis in which each earthquake was linked to the closest fault (or lineament). We then associated specific fault strikes with instrumental earthquakes in order to calculate the tendency of different strike values to be associated with earthquakes.

The distributions of the strikes of all faults and faults nearest to earthquakes (i.e. “active faults”) are presented in Fig. 8. We note that even if a specific fault was associated with multiple earthquakes, it was accounted for only once in the distribution graph in order not to induce bias in the distributions. From the distributions, it can be seen that in the case of all faults in southern Finland, the maxima in strike distributions are found in the strike range of 135–170°, whereas for the group of active faults, two maxima are found for strikes of ca. 95° and 110°. There is thus a clear difference between the two fault populations, suggesting that in southern Finland in general, earthquakes are focused on zones striking E–W and WNW–ESE and, while zones deviating from these strike directions appear to be less active, although they may otherwise be more common fault orientations.

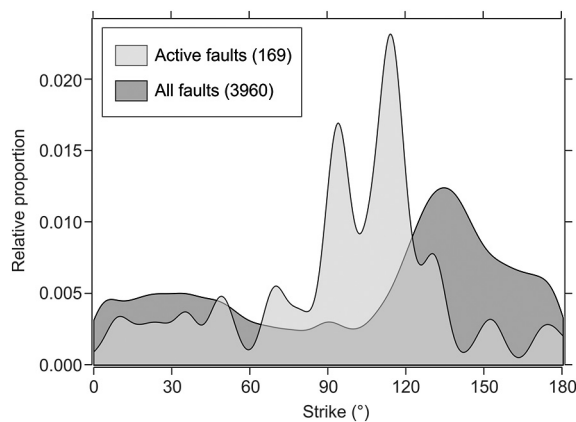


Fig. 8. Distribution of strike values for all faults and active faults in southern Finland.

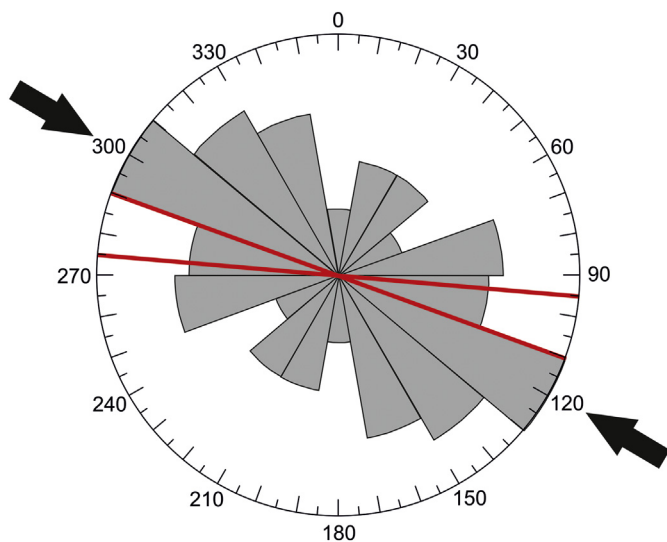


Fig. 9. Orientations of maximum horizontal stresses as given in the World Stress Database (Heidbach et al., 2016), together with the mean strike orientations of active faults (shown with red lines) in this study. (For interpretation of the references to color in this figure legend, the reader is referred to the web version of this article.)

As there are marked differences in the strike orientations for active faults, it is interesting to compare whether these orientations are optimally oriented with respect to the prevailing stress conditions. In order to do this, we extracted the orientations of maximum horizontal stresses from the World Stress Database (Heidbach et al., 2016). The orientations of maximum horizontal stresses (σ_{H}) in southern Finland are illustrated in Fig. 9. These orientations of active faults can be compared with the maximum horizontal stress orientations in southern Finland, which have a mean strike of 123° . It can be seen that the active faults have a small acute angle to the mean maximum horizontal stress orientation, the angle differences being ca. 30° and 15° . The 30° angle is a typical angle difference between σ_{H} and the fault strike if the Mohr-Coulomb failure criterion is assumed and the friction coefficient for the faults is 0.6. This suggests that in general, the WNW-ESE striking structures may be the most prone to reactivation in the current stress regime. The angle difference of 15° is, however, relatively low and would require that the faults are weak and have low friction coefficients. However, we emphasize that it is difficult to draw valid conclusions on potential friction angles based on 2D data alone, and as the stress data have quite large variation around the mean value. Proper assessment of the fault reactivation potential requires that 3D stress and

fault orientation data are available, as the relative magnitudes of the principal stress components may have a significant role in whether a fault may be subject to reactivation (e.g. Morris and Ferrill, 2009). Therefore, we further assessed the potential reactivation conditions of the faults in southern Finland by first acquiring 3D stress data through the inversion of focal mechanisms from southern Finland and then carrying out slip tendency analysis using the stress inversion results and estimated 3D orientations of the faults in the area. Inversion based on focal mechanism data is also considered to represent stresses at seismogenic depth and, as such, is relevant for assessing the reactivation potential.

Korja and Kosonen (2015) compiled all the available focal mechanism data from Finland, and here we focus on the focal mechanisms of earthquakes located in southern Finland. The data set is composed of a total of 29 focal mechanism interpretations and the data are presented in lower hemisphere stereonet in Fig. 10A. The data are composed of a multitude of potential fault plane orientations. The majority, however, display subvertical dips, with NW-SE, NE-SW and ENE-WSW strike orientations being the most common.

For the inversion of the focal mechanism data we used the software 'WinTensor' (Delvaux and Sperner, 2003). The software computes the best-fitting stress tensor for a given dataset of focal mechanisms using an algorithm that searches for compatible stress tensor solutions for the whole dataset and rejects incrementally incompatible focal mechanism data. The rejected mechanisms can be further run as their own datasets until a stable set of stress tensor solutions is attained. Although more often used for analyzing fault slip data, the software can also be used to assess focal mechanism data (Delvaux and Sperner, 2003). The additional benefit of computing stress tensor inversion from focal mechanism data is that, in addition to acquiring principal stress axis orientations, the method also yields an estimate of the stress ratio $(\sigma_2 - \sigma_3)/(\sigma_1 - \sigma_3)$, i.e. an estimate of the relative magnitudes of the stress axis. As focal mechanism data do not distinguish between the two nodal planes, we ran the inversion by taking both of these planes into account at each instance. Further adjustment of the results would require information of the orientation on the actual fault plane hosting the earthquake.

The results of the inversion of focal mechanisms are given in Fig. 10, which resulted in only one stable solution: a strike-slip regime with a σ_1 axis having a plunge and trend of 07° and 280° , respectively (Fig. 10B), and having a stress ratio of 0.65, which is indicative of a slightly transtensive regime (i.e. a mixture of strike-slip and normal faulting regimes). The data that we were unable to process through inversion are presented in Fig. 10C. The dataset was too heterogeneous to yield any reasonable stress tensor with respect to the number of compatible datasets. The former stress tensor yields stress orientations that are compatible with the generally assumed regional maximum horizontal stress orientation, thus giving further confidence in the results. It should, however, be noted that the inversion is based on a dataset covering a relatively large area, and the results can thus be considered as an average mean stress tensor for this whole area.

With the acquired stress tensors, it then is possible to compute slip tendency patterns for analysis of fault the reactivation potential. The slip tendency is a parameter (TS) that is defined as the ratio between the shear (τ) and normal traction (σ_n) on a fault (Morris et al., 1996), and is a measure of whether the forces on the fault exceed its strength:

$$\text{Ts} = \tau/\sigma_n \quad (1)$$

When the stress state is known, the slip tendency can be computed for any possible orientation. By using the 3D stress state acquired from the inversion of focal mechanism data, the associated slip tendency plot is displayed in Fig. 11A and the values have been scaled from 0 to 1 to highlight the fact that from the inversion, we only obtain relative stress magnitudes. Despite this, however, the slip tendency values allow us to assess the relative reactivation potentials of the faults in our study area. The slip tendency stereoplot shows that in the interpreted stress state,

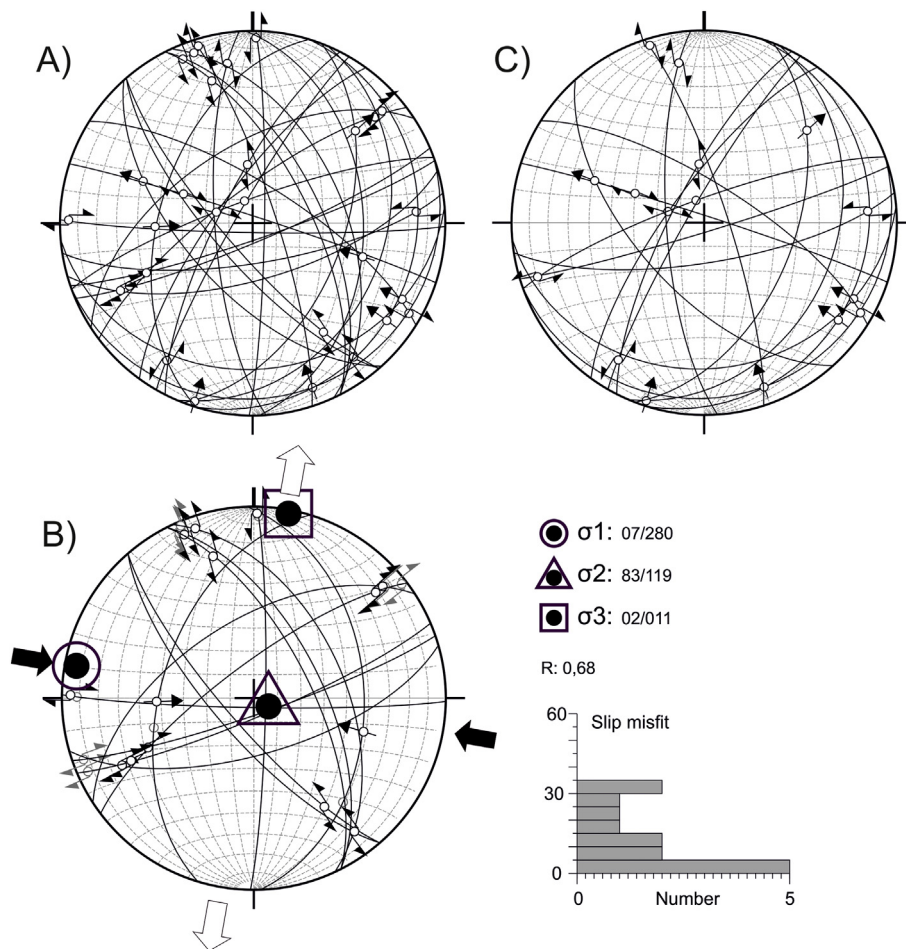


Fig. 10. A) Interpreted fault orientations and associated slip directions and sense of movement from focal mechanism data ($N = 29$). B) Results from the inversion of the focal mechanism data. C) Data could not be processed through inversion.

the highest slip tendency values are attained by vertical to subvertical faults with dip values approximately ranging from 60° to 80° and having strikes in ca. NW-SE and SW-NE orientations. However, for an easier comparison with actual strike data, we also plotted the slip tendency values with respect to the strike orientation (reduced to the interval of 0 – 180°) and dip values, and these are presented in Fig. 11B. As can be seen from the diagram, the maximum slip tendency values are attained by strike directions of about 65° and 130° and for vertical to subvertical structures. With respect to the strike orientations of

southern Finland (Fig. 8), it can be seen that active faults have strikes that are relatively close to the strike value of 130° , which had the maximum slip tendency values. Strike values of about 60° are not very common for the faults in southern Finland, and faults with such strike orientations also do not appear to be very active in the current data set (Fig. 8).

Based on the strike orientations of active faults and the slip tendency analysis, our assessment thus indicates that the approximately NW-SE-striking structures are the most likely candidates to host

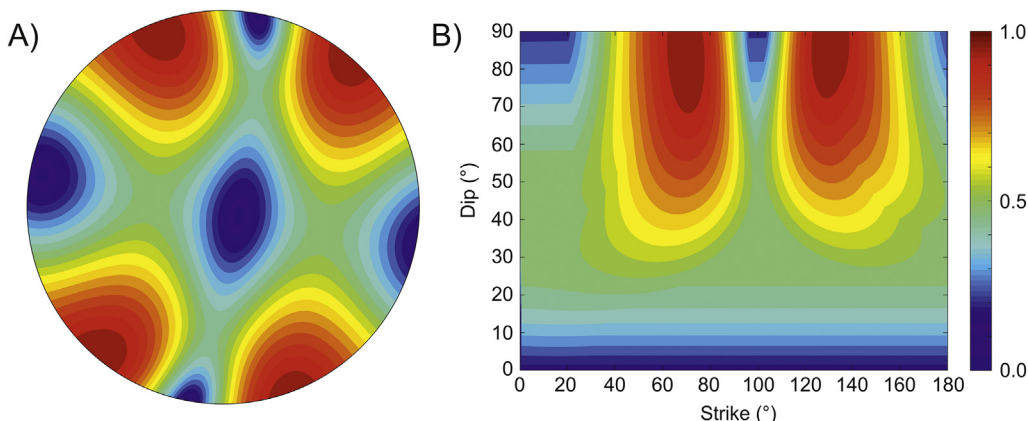


Fig. 11. A) A stereoplot (equal-area, lower hemisphere plot) of relative slip tendency values for each possible orientation for the stress state given in Fig. 10. B) Slip tendency values presented as a function of strike (reduced to the interval of 0 ° to 180 °) and dip orientations.

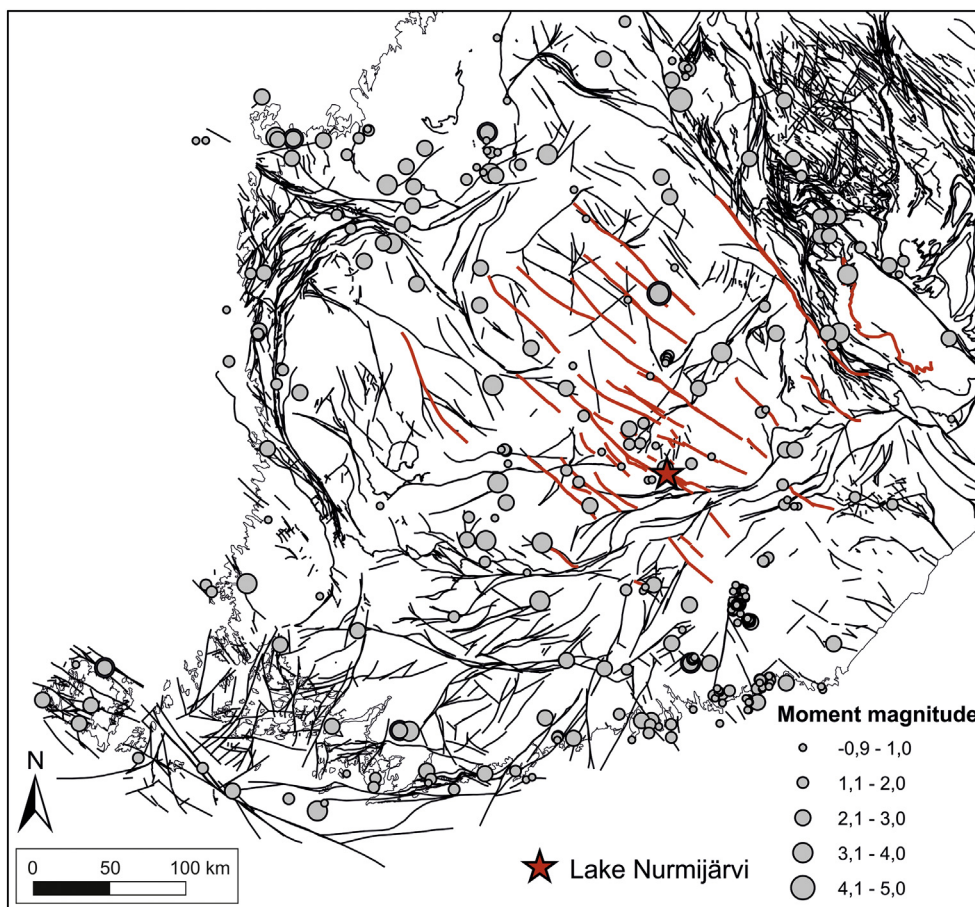


Fig. 12. Faults that are considered to be potential earthquake zones generating the soft-sediment deformation structures (SSDS) observed in the Lake Nurmijärvi section at 7400 cal BP are presented in red. In the assessment, it is assumed that only 40% of the fault length may rupture during an earthquake. (For interpretation of the references to color in this figure legend, the reader is referred to the web version of this article.)

earthquakes in the current stress regime, and furthermore, the most likely earthquake mechanisms are related to the strike-slip setting. This means that in order for the NW–SE-striking structures to reactivate, they need to be vertical to subvertical. Although we do not have specific data for the dip orientations of the faults in our study area, based on the regional assessment carried out by Väisänen and Skyttä (2007) on the shear zones and faults of southern Finland, it is likely that the faults observed in our study area are subvertical in nature.

In the Nurmijärvi area, the most likely candidates for the faults that may have hosted an earthquake are thus the NW–SE-striking structures, of which the most probable candidate is the fault located just south of Lake Nurmijärvi and which has a mean strike orientation of 130° (Fig. 3).

5.3. Estimation of potential moment magnitudes

Due to lack of direct evidence, estimation of the potential moment magnitude of the earthquake that generated the observed deformation structures (SSDS) in the Lake Nurmijärvi section is based on indirect evidence and deduction. In general, an earthquake with a minimum moment magnitude of about $M_w \approx 5.0\text{--}5.7$ and a high enough shaking intensity is required to create extensive SSDS in sediment successions (Obermeier, 1996; Moretti et al., 1999; Monecke et al., 2006). This sets a minimum moment magnitude for the paleoearthquake in the vicinity of Lake Nurmijärvi and also aids in screening the potential earthquake sources, because the earthquake moment magnitudes are also linked to the length and displacement of the earthquake-generating fault (Wells and Coppersmith, 1994; Leonard, 2010). We assessed the potential moment magnitudes for the Nurmijärvi paleoseismic event by using the scaling relationship between fault lengths and moment magnitudes given by Wells and Coppersmith (1994) and Leonard (2010). This was

done by screening out faults that could not have hosted earthquakes larger than $M_w \approx 5$ and then, based on the lengths of the remaining faults in the Nurmijärvi vicinity, we estimated the potential maximum moment magnitudes for the event. As we have no fault displacement data from the study area, the assessment can only rely on fault length data. We also note that as the most likely mechanism for the earthquake is related to strike-slip faulting, the displacement on the faults would be horizontal, and therefore not directly observable as vertical offsets in the Quaternary sediments.

Wells and Coppersmith (1994) and Leonard (2010) have provided the following scaling relationship between the fault surface rupture length (SRL, given in km) and moment magnitudes (M_w) for strike-slip faults, respectively:

$$M_w = 5.16 + 1.12 * \log(SRL) \quad (2)$$

$$M_w = 4.33 + 1.52 * \log(SRL) \quad (3)$$

According to equations, an earthquake with a moment magnitude of $M_w \approx 5$ would require a minimum fault length of about 1–3 km. Irrespective of whether all faults in the study area would satisfy the length criterion, not all of them are within a sufficient distance to produce a high enough intensity of shaking to form the observed SSDS. By assessing a database from Italy, Galli (2000) proposed the following relationship between earthquake magnitude and the maximum distance (R , in km) at which SSDS and liquefaction structures can be formed during an earthquake:

$$M_w = 1.0 + 3.0 \log(R) \quad (4)$$

We thus extended our analysis for the screening of potential faults by first computing the maximum moment magnitudes of the faults in the area, and then by computing their maximum radius for generating liquefaction features through the equation proposed by Galli (2000).

With the above-mentioned constraints, we conducted a spatial query and searched for faults in which (i) the strike is between 110° and 150° (here we account for uncertainties in our analysis by taking a range of $130 \pm 30^\circ$), (ii) the maximum magnitude of the fault is more than $M_w \approx 5$, and (iii) the distance computed from the potential maximum magnitude to Lake Nurmijärvi is less than R as given in Eq. (4). The results of this screening are presented in Fig. 12. We note that the approach is prone misinterpretation, as it is unlikely that all the zones would have ruptured for their entire length in one event, as we have assumed here. For example, Hutchings et al. (2017) suggested that fault rupture often takes place within 10–40% of the total fault area. If we consider that 40% of the total fault length would be a valid estimate for the rupture length in the vicinity of Lake Nurmijärvi, we can further screen down the potential source zones. Screening carried out with this further constraint is illustrated in Fig. 12, showing that the number potential candidate source zones have decreased quite dramatically. Although we cannot exactly pinpoint the source zone, we consider that the weak zone located directly south of Lake Nurmijärvi is still the most potential candidate for the paleoearthquake at 7400 cal BP. This interpretation is supported by the fact that this zone and its immediate surrounding area also have a small cluster of earthquakes compared with the other screened zones. This indicates that this particular zone and other nearby zones are presently active and may also have been so in the past.

When potential maximum moment magnitudes are interpreted for the Nurmijärvi 7400 cal BP paleoseismic event, they reveal an earthquake of $M_w \approx 5.1$ –6.9, assuming that 40% of the potential rupture areas can be considered as a valid approach. If we allow rupturing in a single event for the whole fault length, the estimates vary from $M_w \approx 5.1$ to 7.7. If only the fault south of Nurmijärvi is considered, which has an approximate length of 100 km and which we consider as the most viable source fault for the earthquake, the length-based estimate for that specific zone would yield a maximum moment magnitude estimate of $M_w \approx 7.3$ –7.4, or $M_w \approx 6.8$ –7.0 if only 40% of the rupture length is considered.

5.4. The Nurmijärvi event and Fennoscandian paleoseismicity

There are few published findings on postglacial earthquakes from southern Finland as most of the known postglacial faults are located in northern Finland. Hutri et al. (2007), however, interpreted disturbed sedimentary structures in a marine sequence offshore near Olkiluoto to be seismically-induced features and dated the event at 10,200–10,650 cal BP (Fig. 1). They could not provide estimations of potential moment magnitudes, but noted that the deformation structures were aligned in NW–SE-striking topographic depressions and that the maximum observed displacements were in the range of 2 m. This would account for moment magnitudes in the range of $M_w \approx 7.0$ –7.3 for strike-slip faults (Wells and Coppersmith, 1994), which are thus comparable with the results of the present study. Virtasalo et al. (2007) document displacements of similar size from the Archipelago Sea, which were formed at 10,300 and 11,100 cal BP. Palmu et al. (2015) documented a previously unknown postglacial fault in the Lauhavuori region in southern Finland offsetting glacial sediments and shoreline ridges, which made it possible to delineate the age of the fault to 9500 cal BP. Palmu et al. (2015) did not estimate the potential magnitudes associated with this fault, but the observed vertical maximum offset of the scarp (about 2 m) would indicate a potential maximum moment magnitude in the range of $M_w \approx 6.8$ (Wells and Coppersmith, 1994), assuming that the fault is a reverse fault, as suggested by the offset structure and by the orientation of the zone, which is striking in a NE–SW direction.

From a more extensive geographical perspective, the estimated maximum moment magnitudes of the postglacial faults in northern Finland, Sweden, and Norway generally range from $M_w \approx 6.5$ –8.0 (Lagerbäck, 1990; Arvidsson, 1996; Olesen et al., 2004; Lagerbäck and

Sundh, 2008; Jakobsson et al., 2014; Lund et al., 2017; Ojala et al., 2017a, 2017b), with the postglacial faults in Finland being constrained to maximum moment magnitudes of $M_w \approx 6.5$ –7.5 (Olesen et al., 2004; Sutinen et al., 2014a, 2014b; Ojala et al., 2017b). The ages of the postglacial earthquakes in northern Scandinavia are, however, generally poorly constrained due to the lack of appropriate dating methods and the estimated ages are most often based on either stratigraphic evidence or the dating of landslides thought to be associated with postglacial earthquake activity. In Sweden and Norway, the available dating indicates that known PGFs (Pärvie, Lansjärv, Sorsele, Burträsk, Merasjärv, Röjnret, Soursapakka, Laisvall, Lillsjöhögen and Ismunden, Bollnäs, Stuoragurra) were formed and/or were active during or soon after the deglaciation of these areas, generally between 9500 and 10,500 cal BP (e.g. Lagerbäck, 1990; Stewart et al., 2000; Lagerbäck and Sundh, 2008; Olesen et al., 2013; Berglund and Dahlström, 2015; Mikko et al., 2015; Smith et al., 2014, 2017; Lund et al., 2017).

In Finland, the Suasselkä, Pasmajärvi, Ruokojärvi, and Venejärvi fault ruptures have been interpreted as postglacial faults, but with uncertain timing (Kujansuu, 1972; Stewart et al., 2000; Olesen et al., 2013). According to Sutinen et al. (2014a), the Palojärvi, Paatsikkajoki, and Kultima faults were probably formed subglacially and soon after deglaciation some 10,000 cal BP. Sutinen et al. (2018) also reported seismically-induced subglacial deposits in the Kuusamo area of SE Finnish Lapland that were probably formed during the early Holocene at around 11,500 cal BP. More recently, Ojala et al. (submitted) suggested by analyzing the ages of landslides associated with postglacial faults that, in contrast to what has previously been thought, postglacial faulting in northern Finland has taken place in several episodes. These episodes occurred at 9000–11,000 cal BP, 5000–6000 cal BP, and 1000–3000 cal BP, suggesting more continuous seismic activity throughout the Holocene than previously published. The observations from this study extend this catalogue by identifying a new event in southern Finland at 7400 cal BP and showing that a high-magnitude seismic event took place 3500 years after the deglaciation and further supporting the notion of more continuous postglacial seismic activity during the Holocene. We note that based on the Lake Nurmijärvi sediment section, there is no evidence of repeated high-magnitude seismic events in this area indicating that lithospheric stress release took place a single event. The results from our study also suggest that strike-slip faulting may be a more important mechanism for the generation of postglacial faults as well as for the present day earthquakes in southern Finland than reverse faulting, which has been shown to be a more viable mechanism for the postglacial faults in northern Scandinavia (e.g. Wu et al., 1999; Lund, 2005; Lund et al., 2009). This observation should be accounted for in the assessment of long-term seismic hazards. In the Lake Nurmijärvi case, however, we cannot directly identify the earthquake-generating source fault that generated the observed deformation structures, and more fieldwork is needed to determine which fault or faults were active in southern Finland during the postglacial period. More detailed pinpointing of the actual source fault would require regional assessment of the distribution of disturbed lake sediments and trenching of potential faults in the area. The methodology presented here does however provide a way to delineate potential source areas for paleoseismic events inferred from soft sediment deformation structures, assuming that information of stress state and regional faults are available.

6. Conclusions

A well-dated varved sediment section from Lake Nurmijärvi provides evidence of paleoseismicity in southern Finland at around 7400 cal BP. By screening the potential earthquake-generating faults in southern Finland based fault stability analysis, we were able to estimate that the maximum earthquake moment magnitudes associated with the Lake Nurmijärvi event may have been in the range of $M_w \approx 5.1$ –6.9, if

we assume realistic 40% rupture scenarios, or up to $M_w \approx 5.1\text{--}7.7$ if more conservative scenarios are considered. These observations thus point to a relatively high-magnitude postglacial event in southern Finland that took place 3500 years after the deglaciation of the Lake Nurmijärvi area.

The observations of postglacial earthquakes in southern Finland have so far been sporadic from the Gulf of Bothnia area (Hutri et al., 2007), northern Baltic Sea (Hutri and Kotilanen, 2007), Archipelago Sea (Virtasalo et al., 2007) and in the Lauhavuori region (Palmu et al., 2015). Even systematic LiDAR DEM screening in Finland has not revealed significant evidence of postglacial fault ramps in the southern part of the country and most of the known postglacial earthquakes are located in northern Scandinavia, relatively far from the study area of this paper. Possibly the thicker cover of postglacial fine-grained sediments levels the topography in southern Finland and results in the underrepresentation of fault ramps in the LiDAR DEM. The age of the Lake Nurmijärvi event further indicates that high-magnitude seismic activity was not restricted to a relatively short period after deglaciation and period of maximum rebound, but the period of seismic activity was longer than previously thought. This notion is also supported by the recent findings of Ojala et al. (submitted), who, by dating landslides associated with postglacial faults, showed that Holocene postglacial faulting in northern Finland was more continuous than has previously been thought. By assessing the orientations of faults active during the present-day and using available focal mechanism data, our results further suggest that strike-slip faulting may be a more important mechanism for the generation of postglacial faults in southern Finland than reverse faulting, which should be accounted for in the assessment of long-term seismic hazards.

Acknowledgements

This paper is a contribution of the ‘Postglacial faults and dynamics’ project between GTK (# 50402-20086) and Posiva. Olli Halonen and Vanessa Liedtke are thanked for assisting during sediment coring and analysis and Jyrki Hämäläinen for treating of sub-bottom profiles. This work was supported by the Academy of Finland via RAMI infrastructure project (#293109).

References

- Ahjos, T., Uski, M., 1992. Earthquakes in northern Europe in 1375–1989. *Tectonophysics* 207, 1–23.
- Allen, J.R.L., 1982. *Sedimentary Structures: Their Character and Physical Basis*. Elsevier, Amsterdam.
- Arvidsson, R., 1996. Fennoscandian earthquakes: whole crustal rupturing related to postglacial rebound. *Science* 274, 744–746.
- Beck, C., 2009. Late Quaternary lacustrine paleo-seismic archives in north-western Alps: examples of earthquake-origin assessment of sedimentary disturbances. *Earth Sci. Rev.* 96, 327–344.
- Berglund, M., Dahlström, N., 2015. Post-glacial fault scarps in Jämtland, central Sweden. *GFF* 37, 339–343.
- Bouma, A.H., 1962. *Sedimentology of Some Flysch Deposits: A Graphic Approach to Facies Interpretation*. Elsevier, Amsterdam (168 pp).
- Carillo, E., Beck, C., Audemard, F.A., Moreno, E., Ollarves, R., 2008. Disentangling Late Quaternary climatic and seismo-tectonic controls on Lake Mucubají sedimentation (Mérida Andes, Venezuela). *Palaeogeogr. Palaeoclimatol. Palaeoecol.* 259, 284–300.
- Deike, R.G., Granina, L., Callender, E., McGee, J.J., 1997. Formation of ferric iron crusts in Quaternary sediments of Lake Baikal, Russia, and implications for paleoclimate. *Mar. Geol.* 139, 21–46.
- Delvaux, D., Sperner, B., 2003. Stress tensor inversion from fault kinematic indicators and focal mechanism data: the TENSOR program. In: Nieuwland, D. (Ed.), *New Insights Into Structural Interpretation and Modelling*. Geological Society, London, Special Publications 212pp. 75–100.
- Doughty, M., Eyles, N., Eyles, C., 2013. High-resolution seismic reflection profiling of neotectonic faults in Lake Timiskaming, Timiskaming Graben, Ontario-Quebec, Canada. *Sedimentology* 60, 983–1006.
- Galli, P., 2000. New empirical relationships between magnitude and distance for liquefaction. *Tectonophysics* 324, 169–187.
- Gracia, E., Lamarche, G., Nelson, H., Pantosti, D., 2013. Preface: marine and lake Paleoseismology. *Nat. Hazards Earth Syst. Sci.* 13, 3469–3478.
- Haltia-Hovi, E., Saarinen, T., Kukkonen, M., 2007. A 2000-year record of solar forcing on varved lake sediment in eastern Finland. *Quat. Sci. Rev.* 26, 678–689.
- Heidbach, O., Rajabi, M., Reiter, K., Ziegler, M., WSM Team, 2016. World Stress Map Database Release 2016. GFZ Data Services.
- Hökmärt, H., Fält, B., 2014. Approach to assessing the stability of Olkiluoto deformation zones during a glacial cycle. In: Posiva Working Report WR 2013-37. Posiva Oy, Eurajoki.
- Hutchings, L., Mert, A., Fahjan, Y., Novikova, T., Golara, A., Miah, M., Fergany, E., Foxall, W., 2017. Physics-based hazard assessment for critical structures near large earthquake sources. *Pure Appl. Geophys.* 174, 3635–3662.
- Hutri, K.-L., Kotilanen, A., 2007. An acoustic view into Holocene palaeoseismicity offshore southwestern Finland, Baltic Sea. *Mar. Geol.* 238, 45–59.
- Hutri, K.-L., Heinsalu, A., Kotilanen, A., Ojala, A.E.K., 2007. Dating early Holocene palaeoseismic event(s) in the Gulf of Bothnia, Baltic Sea. *Boreas* 36, 56–64.
- Jakobsson, M., Björck, S., O'Regan, M., Flodén, T., Greenwood, S.L., Swärd, H., 2014. Major earthquake at the Pleistocene-Holocene transition in Lake Vättern, southern Sweden. *Geology* 42, 379–382.
- Korja, A., Kosonen, E., 2015. Seismotectonic Framework and Seismic Source Area Models in Fennoscandia, Northern Europe. Institute of Seismology, University of Helsinki (Report S-63, 268 pp).
- Kujansuu, R., 1972. On landslides in Finnish Lapland. *Bull. Geol. Surv. Finland* 256 (22 pp).
- Kukkonen, I., Olesen, O., Ask, M.V.S., PFDP Working Group, 2010. Postglacial faults in Fennoscandia: targets for scientific drilling. *GFF* 132, 71–81.
- Lagerbäck, R., 1990. Late Quaternary faulting and paleoseismicity in northern Fennoscandia, with particular reference to the Lansjärv area, northern Sweden. *Geol. Fören. Stockh. Förh.* 112, 333–354.
- Lagerbäck, R., Sundh, M., 2008. Early Holocene faulting and paleoseismicity in northern Sweden. In: Geological Survey of Sweden, Research Paper C. 836 (80 pp).
- Lagerbäck, R., Witschard, F., 1983. Neotectonics in Northern Sweden—geological investigations. In: SKBF/KBS Technical Report 83–58. Svensk Kärnbränslehantering AB, Stockholm (58 pp).
- Lajeunesse, P., Sinkunas, B., Morissette, A., Normandeau, A., Joyal, G., St-Onge, G., Locat, J., 2017. Large-scale seismically-induced mass-movements in a former glacial lake basin: lake Témiscouata, northeastern Appalachians (eastern Canada). *Mar. Geol.* 384, 120–130.
- Leonard, M., 2010. Earthquake fault scaling: self-consistent relating of rupture length, width, average displacement, and moment release. *Bull. Seismol. Soc. Am.* 100, 1971–1988.
- Lijklema, L., 1980. Interaction of orthophosphate with iron(III) and aluminium hydroxides. *Environ. Sci. Technol.* 14, 537–541.
- Lindblom, E., Lund, B., 2011. Focal mechanisms and the state of stress along the Pärvie end-glacial fault, northern Sweden. In: Lindblom, E. (Ed.), *Micro-earthquake Study of End-glacial Faults in Northern Sweden*. University of Uppsala, Sweden (PhD thesis in seismology).
- Lund, B., 2005. Effects of deglaciation on the crustal stress field and implications for endglacial faulting: a parametric study of simple Earth and ice models. In: SKBF/KBS Technical Report 05-04. Swedish Nuclear Fuel and Waste Management Co, Stockholm (68 pp).
- Lund, B., Schmidt, P., Hieronymus, C., 2009. Stress evolution and fault stability during the Weichselian glacial cycle. In: SKBF/KBS Technical Report 09-15. Swedish Nuclear Fuel and Waste Management Co, Stockholm (106 pp).
- Lund, B., Roberts, R., Smith, C.A., 2017. Review of paleo-, historical and current seismicity in Sweden and surrounding areas with implications for the seismic analysis underlying SKI report 92:3. In: Strål säkerhets myndigheten. 35 Swedish Radiation Safety Authority (68 pp, report 2017).
- Luoto, T.P., Ojala, A.E.K., 2017. Meteorological validation of chironomids as a paleo-temperature proxy using varved lake sediments. *The Holocene* 27, 870–878.
- Malehmir, A., Andersson, M., Mehta, S., Brodin, B., Munier, R., Place, J., Maries, G., Smith, C., Kamm, J., Bastani, M., Mikko, H., Lund, B., 2015. Post-glacial reactivation of the Bollnäs fault, central Sweden. *Solid Earth Discuss.* 7, 2833–2874.
- Mikko, H., Smith, C., Lund, B., Ask, M.V., Munier, R., 2015. LiDAR-derived inventory of post-glacial fault scarps in Sweden. *GFF* 137, 334–338.
- Moernaut, J., Van Daele, M., Heirman, K., Fontijn, K., Strasser, M., Pino, M., Urrutia, R., De Batist, M., 2014. Lacustrine turbidites as a tool for quantitative earthquake reconstruction: new evidence for a variable rupture mode in south central Chile. *J. Geophys. Res. Solid Earth* 119, 1607–1633.
- Monecke, K., Anselmetti, F.S., Becker, A., Schnellmann, M., Sturm, M., Giardini, D., 2006. Earthquake-induced deformation structures in lake deposits: a Late Pleistocene to Holocene paleoseismic record for Central Switzerland. *Eclogae Geol. Helv.* 99, 343–362.
- Moretti, M., Alfaro, P., Caselles, O., Canas, J.A., 1999. Modelling seismites with a digital shaking table. *Tectonophysics* 304, 369–383.
- Morris, A.P., Ferrill, D.A., 2009. The importance of the effective intermediate principal stress ($\sigma'2$) to fault slip patterns. *J. Struct. Geol.* 31, 950–959.
- Morris, A., Ferrill, A., Henderson, D.B., 1996. Slip tendency analysis and fault reactivation. *Geology* 24, 275–278.
- Mortimer, C.H., 1942. The exchange of dissolved substances between mud and water in lakes. *J. Ecol.* 30, 147–201.
- Munier, R., Fenton, C., 2004. Current understanding and directions for future studies. In: Munier, R., Hökmärt, H. (Eds.), *Respect Distances: Rationale and Means of Computation*. Swedish Nuclear Fuel and Waste Management Co., Stockholm, pp. 157–218 (Report R-04-17).
- Nevanlinna, H., 1979. The geomagnetic field and its secular variation in Finland and nearby countries. *J. Geophys.* 46, 201–216.
- Obermeier, S.F., 1996. Use of liquefaction-induced features for paleoseismic analysis – an overview of how seismic liquefaction features can be distinguished from other features and how their regional distribution and properties of source sediment can be

- used to infer the location and strength of Holocene paleo earthquakes. *Eng. Geol.* 44, 1–76.
- Ojala, A.E.K., Alenius, T., 2005. 10,000 years of interannual sedimentation recorded in the Lake Nautajärvi (Finland) clastic-organic varves. *Palaeogeogr. Palaeoclimatol. Palaeoecol.* 219, 285–302.
- Ojala, A.E.K., Tiljander, M., 2003. Testing the fidelity of sediment chronology: comparison of varve and paleomagnetic results from Holocene lake sediments from central Finland. *Quat. Sci. Rev.* 22, 1787–1803.
- Ojala, A.E.K., Saarinen, T., Salonen, V.-P., 2000. Preconditions for the formation of annually laminated lake sediments in southern and central Finland. *Boreal Environ. Res.* 5, 243–255.
- Ojala, A.E.K., Heinsalu, A., Saarnisto, M., Tiljander, M., 2005. Annually laminated sediments date the drainage of the Ancylus Lake and early Holocene shoreline displacement in central Finland. *Quat. Int.* 130, 63–73.
- Ojala, A.E.K., Palmu, J.-P., Åberg, A., Åberg, S., Virkki, H., 2013. Development of an ancient shoreline database to reconstruct the Litorina Sea maximum extension and the highest shoreline of the Baltic Sea basin in Finland. *Bull. Geol. Soc. Finl.* 85, 127–144.
- Ojala, A.E.K., Mattila, J., Ruskeeniemi, T., Palmu, J.-P., Lindberg, A., Hänninen, P., Sutinen, R., 2017a. Postglacial seismic activity along the Isovaara–Riiikonkumpu fault complex. *Glob. Planet. Chang.* 157, 59–72.
- Ojala, A.E.K., Mattila, J., Markovaara-Koivisto, M., Ruskeeniemi, T., Palmu, J.-P., Sutinen, R., 2017b. Distribution and morphology of landslides in northern Finland – analysis of postglacial seismic activity. *Geomorphology* (in press). <https://doi.org/10.1016/j.geomorph.2017.08.045>.
- Ojala, A.E.K., Luoto, T.P., Virtasalo, J.J., 2017c. Establishing a high-resolution surface sediment chronology with multiple dating methods – testing ^{137}Cs determination with Nurmijärvi clastic-biogenic varves. *Quat. Geochronol.* 37, 32–41.
- Ojala, A.E.K., Markovaara-Koivisto, M., Middleton, M., Ruskeeniemi, T., Mattila, J., Sutinen, R., 2018. Dating of paleolandslides in western Finnish Lapland. *Earth Surf. Process. Landf.* <http://dx.doi.org/10.1002/esp.4408>. (in press).
- Olesen, O., Henkel, H., Lile, O.B., Mauring, E., Rønning, J.S., 1992. Geophysical investigations of the Stuoragurra postglacial fault, Finnmark, northern Norway. *J. Appl. Geophys.* 29, 95–118.
- Olesen, O., Blikra, L.H., Braathen, A., Dehls, J.F., Olsen, L., Rise, L., Roberts, D., Riis, F., Paleide, J.I., Anda, E., 2004. Neotectonic deformation in Norway and its implications: a review. *Nor. J. Geol.* 84, 3–34.
- Olesen, O., Bungum, H., Dehls, J., Lindholm, C., Pascal, C., Roberts, D., 2013. Neotectonics, seismicity and contemporary stressfield in Norway—mechanisms and implications. In: Olsen, L., Fredin, O., Olesen, O. (Eds.), *Quaternary Geology of Norway*. Geological Survey of Norway, Special Publication 13pp. 145–174.
- Owen, G., Moretti, M., Alfaro, P., 2011. Recognising triggers for soft-sediment deformation: current understanding and future directions. *Sediment. Geol.* 235, 133–140.
- Palmu, J.-P., Ojala, A.E.K., Ruskeeniemi, T., Sutinen, R., Mattila, J., 2015. LiDAR DEM detection and classification of postglacial faults and seismically-induced landforms in Finland: a paleoseismic database. *GFF* 137, 344–352.
- Remberg, I., 1982. Varved lake sediments/geochronological records of the Holocene. *Geol. För. Stockh. Förh.* 104, 275–279.
- Saarni, S., Saarinen, T., Dulski, P., 2016. Between the North Atlantic Oscillation and the Siberian High: a 4000-year snow accumulation history inferred from varved lake sediments in Finland. *The Holocene* 26, 423–431.
- Saarnisto, M., 1971. The upper limit of the Flandrian transgression of Lake Päijänne. In: *Societas Scientiarum Fennica, Commentationes Physico-mathematicae*. 41. pp. 149–170.
- Sauramo, M., 1923. Studies on the Quaternary varve sediments in southern Finland. *Comm. Géol. Fin. Bull.* 60, 1–164.
- Seilacher, A., 1969. Fault-graded beds interpreted as seismites. *Sedimentology* 13, 155–159.
- Shanmugam, G., 2017. Global case studies of soft-sediment deformation structures (SSDS): definitions, classifications, advances, origins, and problems. *J. Palaeogeogr.* 6, 251–320.
- Shilts, W.W., Clague, J.J., 1992. Documentation of earthquake-induced disturbance of lake sediments using subbottom acoustic profiling. *Can. J. Earth Sci.* 29, 1018–1042.
- Sims, J.D., 1973. Earthquake-induced structures in sediments of Van Norman Lake, San Fernando, California. *Science* 182, 161–163.
- Smith, C., Sundh, M., Mikko, H., 2014. Surficial geologic evidence for early Holocene faulting and seismicity. *Int. J. Earth Sci.* 103, 1711–1724.
- Smith, C.A., Nyberg, J., Bergman, B., 2017. Comparison between hydroacoustical and terrestrial evidence of glacially induced faulting, Lake Voxsjön, central Sweden. *Int. J. Earth Sci.* <http://dx.doi.org/10.1007/s00531-017-1479-4>.
- Snowball, I., Zillén, L., Ojala, A., Saarinen, T., Sandgren, P., 2007. FENNOSTACK and FENNORPIS: varve dated Holocene palaeomagnetic secular variation and relative palaeointensity stacks for Fennoscandia. *Earth Planet. Sci. Lett.* 255, 106–116.
- Stewart, I.S., Sauber, J., Rose, J., 2000. Glacio-seismotectonics, ice sheets, crustal deformation and seismicity. *Quat. Sci. Rev.* 19, 1367–1389.
- Stow, D.A.V., Shanmugam, G., 1980. Sequence of structures in fine-grained turbidites: comparison of recent deep-sea and ancient flysch sediments. *Sediment. Geol.* 25, 23–42.
- Strasser, M., Monecke, K., Schnellman, M., Anselmetti, F., 2013. Lake sediments as natural seismographs: a compiled record of Late Quaternary earthquakes in Central Switzerland and its implications for Alpine deformation. *Sedimentology* 60, 319–341.
- Strömbärg, B., 2005. Clay varve chronology and deglaciation in SW Finland. In: *Annales Academiae Scientiarum Fennicae, Geologica-Geographica*. 167 (47 pp).
- Sutinen, R., Hyvönen, E., Middleton, M., Ruskeeniemi, T., 2014a. Airborne LiDAR detection of postglacial faults and Pulju moraine in Palojärvi, Finnish Lapland. *Glob. Planet. Chang.* 115, 24–32.
- Sutinen, R., Hyvönen, E., Kukkonen, I., 2014b. LiDAR detection of paleolandslides in the vicinity of the Suasselkä posglacial fault, Finnish Lapland. *Int. J. Appl. Earth Obs. Geoinf.* 27, 91–99.
- Sutinen, R., Hyvönen, E., Middleton, M., Airo, M.-L., 2018. Earthquake-induced deformations on ice-stream landforms in Kuusamo, eastern Finnish Lapland. *Glob. Planet. Chang.* 160, 46–60.
- Svendsen, J.I., Alexanderson, H., Astakhov, V.I., Demidov, I., Dowdeswell, J.A., Funder, S., Gataullin, V., Henriksen, M., Hjort, C., Houmark-Nielsen, M., Hubbard, H.W., Ingólfsson, Ó., Jakobsson, M., Kjaer, K.H., Larsen, E., Lokrantz, H., Lunkka, J.P., Lyså, A., Mangerud, M., Matiouchkov, A., Murray, A., Möller, P., Niessen, F., Nikolskaya, O., Polyak, L., Saarnisto, M., Siegert, C., Siegert, M.J., Spielhagen, R., Stein, R., 2004. Late quaternary ice sheet history of northern Eurasia. *Quat. Sci. Rev.* 23, 1229–1271.
- Uski, M., Hyvönen, T., Korja, A., Airo, M.-L., 2003. Focal mechanisms of three earthquakes in Finland and their relation to surface faults. *Tectonophysics* 363, 141–157.
- Väistönen, M., Skyttä, P., 2007. Late Svecofennian shear zones in southwestern Finland. *GFF* 129, 55–64.
- Virtasalo, J.J., Kotilainen, A.T., Räsänen, M.E., Ojala, A.E.K., 2007. Late-glacial and post-glacial deposition in a large, low relief, epicontinental basin: the northern Baltic Sea. *Sedimentology* 54, 1323–1344.
- Vogel, H., Wagner, B., Rosén, P., 2013. Lake floor morphology and sediment architecture of lake Torneträsk, Northern Sweden. *Geogr. Ann. Ser. B* 95, 159–170.
- Wardinski, I., 2007. Geomagnetic secular variation. In: Gubbins, D., Herrero-Bervera, E. (Eds.), *Encyclopedia of Geomagnetism and Paleomagnetism*. Springer, Dordrecht, pp. 346–350.
- Wells, D.L., Coppersmith, K.J., 1994. New empirical relationships among magnitude, rupture length, rupture width, rupture area, and surface displacement. *Bull. Seismol. Soc. Am.* 84, 974–1002.
- Wu, P., Johnston, P., Lambeck, K., 1999. Postglacial rebound and fault instability in Fennoscandia. *Geophys. J. Int.* 139, 657–670.
- Zolitschka, B., Francus, P., Ojala, A.E.K., Schimmelmann, A., 2015. Varves in lake sediments - a review. *Quat. Sci. Rev.* 117, 1–41.